Analyst

Cite this: *Analyst*, 2012, **137**, 4552

www.rsc.org/analyst

PAPER

BSA-templated MnO_2 nanoparticles as both peroxidase and oxidase mimics†

Xing Liu,[a] Qi Wang,[a] Huihui Zhao,[a] Lichun Zhang,[a] Yingying Su[b] and Yi Lv*[a]

Received 27th May 2012, Accepted 30th July 2012
DOI: 10.1039/c2an35700c

Inorganic nanomaterials that mimic enzymes are fascinating as they potentially have improved properties relative to native enzymes, such as greater resistance to extremes of pH and temperature and lower sensitivity to proteases. Although many artificial enzymes have been investigated, searching for highly-efficient and stable catalysts is still of great interest. In this paper, we first demonstrated that bovine serum albumin (BSA)-stabilized MnO_2 nanoparticles (NPs) exhibited highly peroxidase-, oxidase-, and catalase-like activities. The activities of the BSA-MnO_2 NPs were evaluated using the typical horseradish peroxidase (HRP) substrates *o*-phenylenediamine (OPD) and 3,3′,5,5′-tetramethylbenzidine (TMB) in the presence of either hydrogen peroxide or dissolved oxygen. These small-sized BSA-MnO_2 NPs with good dispersion, solubility and biocompatibility exhibited typical Michaelis–Menten kinetics and high affinity for H_2O_2, OPD and TMB, indicating that BSA-MnO_2 NPs can be used as satisfactory enzyme mimics. Based on these findings, BSA-MnO_2 NPs were used as colorimetric immunoassay tags for the detection of goat anti-human IgG in place of HRP. The colorimetric immunoassay using BSA-MnO_2 NPs has the advantages of being fast, robust, inexpensive, easily prepared and with no HRP and H_2O_2 being needed. These water-soluble BSA-MnO_2 NPs may have promising potential applications in biotechnology, bioassays, and biomedicine.

1. Introduction

Natural enzymes with high substrate specificity and high catalytic efficiency[1–4] play central roles in biochemistry and have been extensively studied for more than 200 years. Unfortunately, natural enzymes suffer greatly from their instability, *i.e.*, they are easily denatured, prone to digestion by protease and are difficult to be purified.[5] Accordingly, searching for natural enzyme mimics and/or artificial enzymes with good stability is urgently needed. Inorganic nanomaterials have received considerable attention in catalysis due to their large surface-to-volume ratio.[6,7] Recently, an unexpected finding reported by Yan and co-workers revealed that inorganic nanoparticles (NPs) may be potential enzyme mimics: they found Fe_3O_4 magnetic NPs exhibited intrinsic peroxidase-like activity and successfully displayed the detection of hepatitis B virus (HBV) preS1 and TnI.[8] Afterwards, a variety of inorganic nanomaterials including V_2O_5 nanowires, Pt NPs, Au@Pt nanorods, Au NPs, carbon nanodots, graphene oxide, single-walled carbon nanotubes, CuO NPs, FeTe nanorods, Co_3O_4 NPs, *etc.*, were reported to give similar peroxidase-like properties.[9–22] Simultaneously, polymer-coated CeO_2 NPs, and polyoxometalates have been employed as an oxidase-like biocatalyst for enzyme-linked immunosorbent assay (ELISA).[23,24] These studies show that the nanomaterial-based enzyme mimics take have the advantages of low cost and high stability in catalytic activities and can be potentially used in bioassays and medical diagnostics.

In either horseradish peroxidase (HRP)- or the above artificial enzymes-catalyzed reactions, H_2O_2 is often employed as the oxidant. H_2O_2 is one of the most important chemical molecules involved in biological processes.[25] In routine ELISA kits, HRP–H_2O_2–color substrate systems are typically employed.[26,27] The catalytic mechanism is that the enzyme catalyzes the two-electron reduction of H_2O_2 to H_2O forming an intermediate complex, then the color substrate binds to the complex by a nucleophilic attack, thus allowing the oxidation reaction with a color change *via* eqn (1).[28]

$$SH_2 + H_2O_2 \xrightarrow{HRP} S + 2H_2O \quad (1)$$

From textbook knowledge, we know that MnO_2 can catalyze the decomposition of H_2O_2 in the following way (eqn (2)):

$$2H_2O_2 \xrightarrow{MnO_2} 2H_2O + O_2 \quad (2)$$

It is thus expected that MnO_2 may also exhibit similar peroxidase-like activity, but to our knowledge, no such reports have been evidenced until now. We thus tested the peroxidase-like activity of commercial micrometer-sized MnO_2 powder with

[a]*Key Laboratory of Green Chemistry & Technology, Ministry of Education, College of Chemistry, Sichuan University, Chengdu, Sichuan 610064, China. E-mail: lvy@scu.edu.cn; Fax: +86 28 8541 2798; Tel: +86 28 8541 2798*
[b]*Analytical & Testing Center, Sichuan University, Chengdu, Sichuan 610064, China*

† Electronic supplementary information (ESI) available. See DOI: 10.1039/c2an35700c

o-phenylenediamine (OPD) as the substrate (Fig. S1, ESI†). To our delight, MnO_2 did catalyze the oxidation of OPD by H_2O_2 to produce an orange color, *i.e.*, peroxidase-like activity, but the catalytic efficiency was significantly lower than the former systems and HRP. It is generally recognized that the catalytic efficiency can be greatly improved by decreasing the particle size.[29]

In this regard, protein-templated synthesis of inorganic NPs can give the desired shape, small size and availability of subsequent bioconjugation.[30] Among the proteins, bovine serum albumin (BSA) is the most abundant plasma protein and a model globular protein that is widely used in biomineralization due to its strong affinity towards inorganic salts.[31] In this work, we developed the BSA-directed synthesis of MnO_2 NPs with small size, good dispersion, solubility, and biocompatibility and explored their peroxidase-, oxidase-, and catalase-like activities.

Colorimetric immunoassays using a HRP-labeled secondary antibody have many advantages for the detection of proteins such as being a simple analytical procedure, having a short analysis time, high detection efficiency, low sample volume and low cost. However, some drawbacks need to be improved: HRP often loses its enzymatic activity when denatured; H_2O_2 decomposes upon prolonged storage, and loses its ability to oxidize 3,3′,5,5′-tetramethylbenzidine (TMB) in the presence of HRP. Using biocompatibility, BSA-MnO_2 NPs-labeled antibodies could be obtained that are more stable and a convenient immunoassay method for extensive clinical applications. As a proof of concept, goat anti-human IgG was detected using BSA-MnO_2 NPs in the place of HRP for sensitive colorimetric immunoassay.

2. Experimental

2.1. Reagents

Deionized water with a conductivity of 18.2 MΩ cm^{-1} was used in this experiment from a water purification system (ULUPURE, Chengdu, China). Polystyrene 96-well microtiter plates (468667, NUNC, Denmark) were used to perform the immunoreactions. Human IgG, rabbit anti-goat IgG, goat anti-human IgG, BSA and all the other proteins were purchased from Solarbio Science & Technology Co. Ltd. (Beijing, China). *o*-Phenylenediamine (OPD), 3,3′,5,5′-tetramethylbenzidine (TMB) and horseradish peroxidase (HRP) were purchased from Aokesheng Co. Ltd. (Chengdu, China). 1-Ethyl-3-(3-dimethylaminopropyl)carbodiimide hydrochloride (EDC·HCl) and *N*-hydroxysuccinimide (NHS) were purchased from Aladdin Inc. (Shanghai, China). MnO_2 powder (AR) of 4–7 μm size was purchased from Jinbei Fine Chemistry Co. Ltd. (Tianjin, China). Manganese acetate ($MnAc_2$, M_w = 245.09, AR), sodium hydroxide (NaOH, GR), hydrogen peroxide (H_2O_2, 30%) and all the other reagents were at least of analytical grade and obtained from Kemiou Chemical Reagent Co. Ltd. (Tianjin, China).

2.2. Immunoreaction buffers

The buffers used were as follows: (a) coating buffer, 0.05 mol L^{-1} carbonate/bicarbonate buffer solution, pH 9.6 (dissolve 1.590 g of Na_2CO_3 and 2.930 g of $NaHCO_3$ in 1 L of deionized water); (b) blocking buffer, 3% (w/v, g mL^{-1}) BSA in 0.01 mol L^{-1} sodium phosphate buffered saline, pH 7.4 (PBS, dissolve 1.204 g of $Na_2HPO_4 \cdot 12H_2O$, 0.600 g of $NaH_2PO_4 \cdot 2H_2O$ and 8.766 g of NaCl in 1 L of deionized water); (c) washing buffer, 0.01 mol L^{-1} PBS with 0.05% (v/v) Tween 20 (PBST), pH 7.4, which can be kept at 4 °C for at least 2–3 weeks; (d) NaAc buffer (0.2 mol L^{-1} NaAc solution with HAc adjusting pH 4.0); and (e) 0.2 mol L^{-1} citrate buffer (7.300 g of $Na_2HPO_4 \cdot 2H_2O$ and 4.665 g of citric acid in 500 mL of deionized water).

2.3. Instrumentations

Transmission electron microscopy (TEM), high-resolution transmission electron microscopy (HRTEM), selected-area electron diffraction (SAED), and the energy dispersive X-ray spectroscopy (EDX) of MnO_2 NPs were carried out using a Tecnai G^2 F20 S-TWIN transmission electron microscope at an accelerating voltage of 200 kV (FEI Co., USA). Samples were prepared for analysis by evaporating a drop of aqueous product on a lacey carbon copper TEM grid. Dynamic light scattering (DLS) and zeta potential were performed with a Zetasizer Nano ZS (Malvern Co., UK) and the circular dichroism spectrum (CD) was recorded with a Model 400 circular dichroism spectrometer (AVIA Biomedical Inc., USA). X-Ray photoelectron spectroscopy (XPS) was performed using an XSAM 800 electron spectrometer (Kratos) using monochromatic Mg K_α radiation for analysis of the surface composition and chemical states of the product. The UV-vis absorption spectrum and the photoluminescence spectrum were obtained using a U-2910 UV-vis spectrophotometer and an F-7000 fluorescence spectrophotometer (Hitachi Co., Tokyo, Japan). Fourier Transform Infrared spectra (FTIR) from 4000 to 400 cm^{-1} were recorded as KBr discs using a Nicolet IS10 FTIR spectrometer (Thermo Inc., USA) for evaluating the encapsulation of MnO_2 NPs within BSA. Thermogravimetry (TG) measurement was carried out in air at a heating rate of 10 °C min^{-1} on an STA449C thermal analyzer (NETZSCH Co., Germany) and a flame atomic absorption spectrometer (FAAS, Zeeman GGX-6, Beijing Geological Instrument Co., China) was used for the detection of the amount of manganese element in solution.

2.4. Preparation of BSA-MnO_2 NPs

In a typical process, 25 mg BSA with 10 mL of 0.01 mol L^{-1} PBS buffer was transferred into a 20 mL reaction flask, then 50 μL of 100 mmol L^{-1} $MnAc_2$ aqueous solution was added. The mixed solution of Mn^{2+}–BSA emulsion was kept stirring for 2 min at room temperature, and then 50 μL of 1 mol L^{-1} NaOH aqueous solution was added to the as-prepared solutions. After NaOH addition, the color of the solution immediately changed to an orange color. Finally, the BSA-MnO_2 NPs were obtained after stirring for 6–8 h. The solution was then dialyzed in double distilled water for 48 h and centrifuged at 18 500 rpm for 30 min to remove unreacted $MnAc_2$ and NaOH. The final solution was stored at 4 °C in a refrigerator when not in use.

2.5. Preparation of human IgG-conjugated MnO_2 NPs

0.5 mL purified BSA-MnO_2 NPs solution were mixed with 1.5 mL PBS buffer, then 1 mg EDC·HCl and 1.5 mg NHS aqueous solution were added.[32] 15 min later, 50 μg human IgG

was added and incubated for 2 h. After centrifugation at 18 500 rpm for 30 min, the human IgG-conjugated MnO_2 NPs were used for goat anti-human IgG detection in the immunoassay.

2.6. Immunoassay principles

The schematic diagram of the sandwich-type immunoassay for the detection of goat anti-human IgG is shown later in Fig. 5a. Initially, polystyrene 96-well microtiter plates were coated with 200 μL of rabbit anti-goat IgG (diluted to 10 μg mL^{-1} solution with coating buffer) *via* physical adsorption between hydrophobic groups of antibody molecules and polystyrene in the course of incubation at 4 °C overnight. The unbound rabbit anti-goat IgG solution was washed away three times with 350 μL washing buffer. Then the wells were incubated with 300 μL blocking buffer for 1 h at 37 °C to minimize non-specific adsorption of the goat anti-human IgG. After excess BSA was washed away three times with 350 μL washing buffer, different concentrations of 200 μL goat anti-human IgG solution were pipetted into the wells for 1 h incubation at 37 °C and followed by addition of 200 μL human IgG-conjugated MnO_2 NPs for 1.5 h incubation at 37 °C. Unbound goat anti-human IgG and human IgG-conjugated MnO_2 NPs were washed three times with 350 μL washing buffer and three times with 350 μL deionized water. Each well was dissolved with 200 μL of 5.0 mmol L^{-1} OPD in NaAc buffer or 200 μL of 2.5 mmol L^{-1} TMB in citrate buffer for 15 min. UV-vis absorption spectrum was used for the determination of the goat anti-human IgG concentration.

3. Results and discussion

3.1. Optimization of the synthesis of BSA-MnO_2 NPs parameters

The UV-vis absorption spectrum was used to investigate the formation of MnO_2 NPs. Firstly, as shown in Fig. S2a, ESI,† when the pH was greater than 11.62, the BSA-Mn^{2+} was mostly transformed into BSA-MnO_2 NPs. Secondly, different reaction temperatures were investigated (Fig. S2b, ESI†). It was found that MnO_2 NPs formed very quickly when the temperature was at the range from 20 °C to 50 °C; a higher temperature, however, could cause BSA inactivation. Thirdly, ionic strength was investigated using different concentrations of NaCl (Fig. S2c, ESI†), and 0.01 mol L^{-1} ionic strength was best due to the solubility of BSA. Lastly, the molar ratio of BSA and Mn^{2+} precursor was critical for controlling the size of the NPs. As shown in Fig. S2d, ESI,† decreasing the concentration of BSA led to the sedimentation of the MnO_2 NPs. Thus, the molar ratio of 3.7 : 100 for BSA and Mn^{2+} precursor, respectively, was used.

3.2. Reaction mechanism

This biomineralization of MnO_2 with BSA may be a multistep process involving Mn(II) binding, oxidation by oxygen, nucleation and crystal growth with uniform orientation. As shown in Fig. 1a, BSA provided amino acid residues for specific affinity with Mn(II). MnO_2 was achieved by oxidation of Mn(II) in air, and the deposition/crystallization of MnO_2 should occur selectively only on the specific sites of BSA. During the process, oxygen was important. When the reaction was bubbled with high purity nitrogen, no MnO_2 NPs were formed, indicating that oxygen may participate in the reaction to form the Mn–O bond. The addition of NaOH was also necessary. No NPs were obtained without NaOH, indicating that pH is very important. As shown in Fig. S3a, ESI,† the characteristic peak of the –OH group band shifted by about 109 cm^{-1} to a higher wave number and amide A′ bands shifted by about 97 cm^{-1} to a lower wave number, suggesting that there might be coordination interaction between Mn^{2+} and the –NH, –OH groups of BSA. During the formation of MnO_2 NPs, the secondary structures of BSA changed from α-helix content to the β-sheet and random coil structures (Fig. S3b, ESI†). Thus, the nature of the amino acids, the amino acid sequence, secondary structure, tertiary structure and spatial conformation of the protein are important aspects for biomineralization.

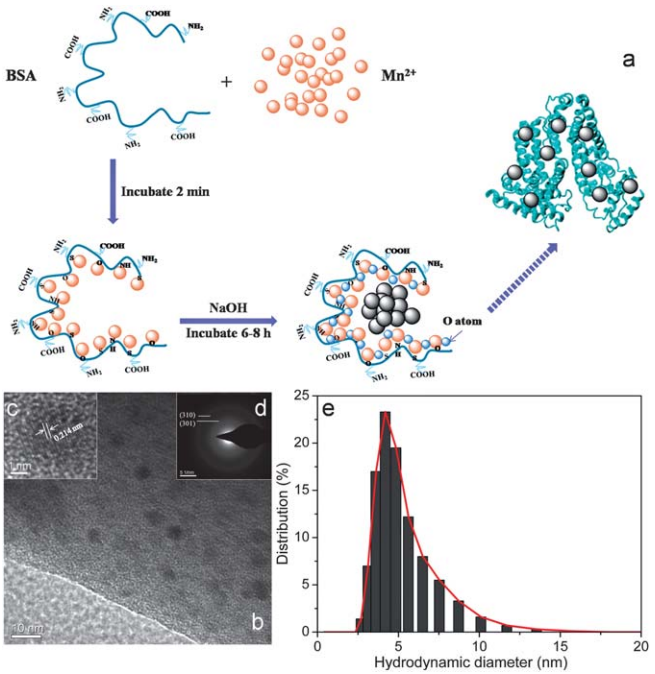

Fig. 1 (a) Schematic of BSA-templated synthesis of MnO_2 NPs; (b) TEM image of BSA-MnO_2 NPs; (c) HRTEM image of BSA-MnO_2 NPs; (d) the SAED pattern in an area including MnO_2 NPs; and (e) the DLS histograms of BSA-MnO_2 NPs.

3.3. Characterization of BSA-MnO_2 NPs

The TEM image (Fig. 1b) and DLS (Fig. 1e) demonstrated that the MnO_2 NPs wrapped in a thin coat of BSA were homogeneous and monodispersed with a narrow size distribution centered at around 4.5 nm and a hydrodynamic diameter of 7.3 nm. Meanwhile, the zeta potential of BSA-MnO_2 NPs was −14.9 mV due to the reaction pH being greater than the isoelectric point of BSA (pI = 4.7). This revealed that the MnO_2 NPs solution had good stability, which is beneficial for its storage, preservation and application. The HRTEM image of Fig. 1c provided further insight into the structure of the NPs. The interplanar distance was about 0.214 nm, which was the same as the interplanar distance between the (3 0 1) planes of γ-MnO_2. SAED (Fig. 1d) showed principally rings of the (3 0 1) and (3 1 0) planes, which

were also consistent with the results of X-ray diffraction (XRD) data of γ-MnO_2 (JCPDS no. 42-1348). As shown in Fig. S4a, ESI,† the compositions of BSA-MnO_2 NPs were of elements carbon, nitrogen, oxygen, sulfur and manganese by EDX. In addition, the element copper was from a lacey carbon copper TEM grid. XPS was also carried out to determine the oxidation state and binding properties of MnO_2. It showed that our samples were composed of elements C 1s 62.6%, O 1s 27.5%, N 1s 6.0% and Mn 2p 3.9%, which coincided with the data from EDX (Fig. S4b, ESI†). As shown in Fig. S4c, ESI,† two intense peaks were observed at 642.4 eV and 653.9 eV, which were assigned to the Mn 2p3/2 and Mn 2p1/2 features of MnO_2. In addition, the presence of MnO_2 could be further confirmed by the O 1s peak at 531.8 eV. As shown in Fig. S4d, ESI,† there were three types of oxygen species in different oxygen-containing functional groups: the oxygen in Mn–O–Mn was at 529.77 eV, the oxygen in Mn–O–H was at 531.14 eV, and the oxygen in H–O–H was at 532.32 eV.[33] Thus, these confirmed that the obtained NPs were MnO_2.

3.4. Characterization of peroxidase-, oxidase- and catalase-like activities of BSA-MnO_2 NPs

Interestingly, the as-synthesized BSA-MnO_2 NPs were found to exhibit peroxidase- and oxidase-like activities, *i.e.*, BSA-MnO_2 could catalyze the oxidation of OPD and TMB in the presence and absence of H_2O_2, respectively. Control experiments showed BSA did not have any appreciable catalytic activity for the oxidation of substrates (Fig. S1, ESI†). Meanwhile, micrometer-sized MnO_2 powder exhibited peroxidase-like activity, but the catalytic efficiency was much lower. Accordingly, the improved intrinsic peroxidase- and oxidase-like activities had arisen from the BSA-MnO_2 NPs.

The peroxidase-like activity of BSA-MnO_2 NPs was investigated with OPD as the substrate. As shown in Fig. 2a, BSA-MnO_2 NPs could oxidize OPD in the absence of H_2O_2 to produce an orange colour (maximum absorbance 450 nm) within 5 min. The absorbance slope of the OPD–MnO_2–H_2O_2 system at 450 nm was much higher than that of the OPD–HRP–H_2O_2 and OPD–MnO_2 systems. This result supported the proposal that BSA-MnO_2 NPs have a higher peroxidase-like activity than HRP. The reaction mechanisms can be described by the equation in Fig. 2b.

Subsequently, the TMB substrate was used to investigate the oxidase-like activity of BSA-MnO_2 NPs in the absence of H_2O_2. It showed that BSA-MnO_2 NPs could catalyze the fast oxidation of TMB in the absence of H_2O_2 to produce a deep blue color (maximum absorbance 652 nm) within 5 min (Fig. 2c). The catalytic efficiency of BSA-MnO_2 NPs was three times higher than micrometer-sized MnO_2 powder, indicating that the smaller the size, the higher the catalytic efficiency. The catalytic reaction rate of TMB oxidation decreased quickly after bubbling with high purity nitrogen. This indicated that the nature of the oxidase-like activity of BSA-MnO_2 NPs for TMB oxidation originated from their catalytic ability to reduce dissolved oxygen (Fig. S6, ESI†). Thus, we presumed that the reaction mechanism of the oxidase-like activity of BSA-MnO_2 NPs can be described by the equation in Fig. 2d.

In addition, the BSA-MnO_2 NPs can reduce the production of OH radicals by catalyzing the decomposition of H_2O_2 in a concentration-dependent manner, indicating that the BSA-MnO_2 NPs have catalase-like activity. On the one hand, terephthalic acid was adopted as a fluorescence probe to evaluate the effects of the BSA-MnO_2 NPs on the OH radical signal intensity, in which terephthalic acid easily reacted with OH to form highly fluorescent 2-hydroxyterephthalic acid. 10 mM H_2O_2, 0.5 mM terephthalic acid and different concentrations of the BSA-MnO_2 NPs were first incubated in 100 mM NaAc buffer (pH 5.0) and exposed to UV light at 365 nm for 20 min. After centrifugation, the solutions were used for fluorometric measurement using an F-7000 fluorescence spectrometer (Fig. S7a, ESI†). As shown in Fig. S7a, ESI,† a gradual decrease of the fluorescence intensity was observed while increasing the concentration of the BSA-MnO_2 NPs, suggesting that the BSA-MnO_2 NPs can reduce the OH radical production by catalyzing the decomposition of H_2O_2 in a concentration-dependent manner. The behavior is similar to that of catalase in the H_2O_2/UV/DMPO system.[10] On the other hand, a YSI 52 dissolved oxygen meter (YSI, America) was used to study oxygen generation as a product of H_2O_2 decomposition by the BSA-MnO_2 NPs. The dissolved oxygen concentration increases as the concentration of BSA-MnO_2 NPs increases (Fig. S7b, ESI†). This result provided direct evidence that the BSA-MnO_2 NPs

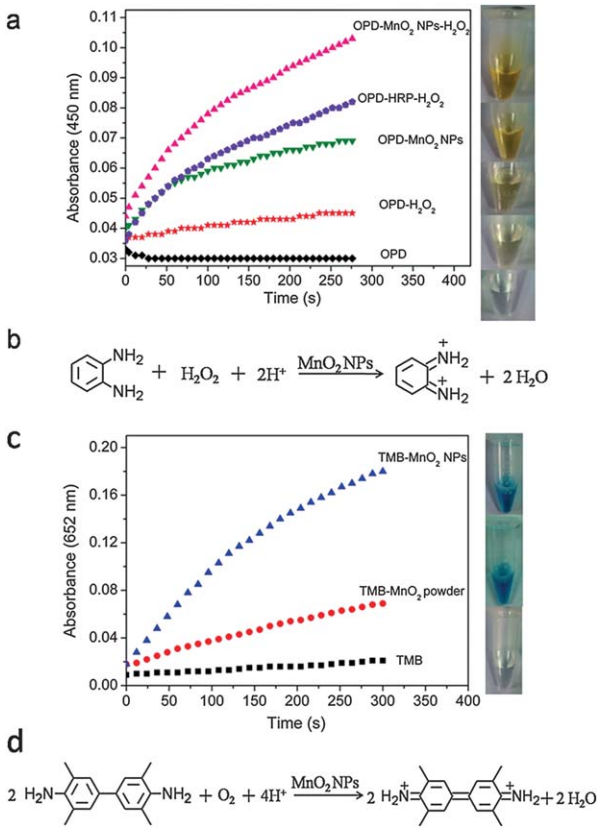

Fig. 2 (a) The time-dependent absorbance changes at 450 nm of OPD with 3.7 μg mL^{-1} BSA-MnO_2 NPs or 3.3 μg mL^{-1} HRP; (b) the corresponding reaction equation for H_2O_2 reduction with OPD; (c) the time-dependent absorbance changes at 652 nm of TMB in the absence of H_2O_2 with 3.7 μg mL^{-1} BSA-MnO_2 NPs or 3.7 μg mL^{-1} micrometer-sized MnO_2 powder; and (d) the corresponding reaction equation by dissolved oxygen with TMB.

exhibit catalase-like activity. The UV-vis absorption spectrum was used to investigate the kinetics of the catalase activity of BSA-MnO_2 NPs and H_2O_2. The data were fitted to the Michaelis–Menten model and the parameter for K_m was −14.31 mM and V_{max} was 4.21 nM s^{-1}.

3.5. Catalytic relative activity of BSA-MnO_2 NPs against pH and temperature

The catalytic relative activity of BSA-MnO_2 NPs is, like HRP, dependent on pH and temperature. Here, we measured the peroxidase- and oxidase-like activities of BSA-MnO_2 NPs while varying the pH from 1.0 to 12.0 and the temperature from 20 °C to 90 °C, and compared the results with the peroxidase-like activity found in HRP over the same range of parameters. The effects of these two parameters on the catalytic relative activity of OPD and TMB oxidation are shown in Fig. S8, ESI.† Not only for OPD, but also for TMB, the optimal pH was *ca.* 4.0 and the optimum temperature was 35 °C. This is because OPD and TMB have a similar structure to diamine, which leads to a poor solubility in a weak base medium. Thus, the pH-dependent catalytic activity was mainly related to the substrates rather than the nanostructures themselves. In addition, the optimization of different types of buffers for OPD and TMB was shown in Fig. S9, ESI.† 0.2 mol L^{-1} NaAc buffer was used for OPD oxidation and 0.2 mol L^{-1} citrate buffer was used for TMB oxidation.

3.6. Stability and kinetic analysis of BSA-MnO_2 NPs

The stability of NPs against aggregation under different harsh conditions is critical to extend their applications. Here, BSA-MnO_2 NPs were found to be stable within alkaline conditions and at temperatures from 20 to 60 °C (Fig. S10, ESI†). Under the optimum conditions, the steady-state kinetics for the catalytic activity of BSA-MnO_2 NPs towards the oxidization of OPD with H_2O_2 (Fig. 3) and TMB with dissolved oxygen (Fig. 4) were determined and typical Michaelis–Menten curves were obtained. For the peroxidase-like activity of BSA-MnO_2 NPs (Table 1), BSA-MnO_2 NPs have a smaller K_m value, indicating that the affinity between OPD and the BSA-MnO_2 NPs is stronger than that between OPD and HRP. This may be due to BSA-MnO_2 NPs, with a small particle size and a high surface area to volume ratio, being more active catalysts, thus giving a lower K_m, higher V_{max}, and a higher enzyme activity than HRP. As shown in Fig. 3e and f, the slopes of the lines are parallel, which is characteristic of a ping-pong mechanism. This indicates that the mechanism is that BSA-MnO_2 NPs reacts with H_2O_2 forming an intermediate peroxo species, and the OPD substrate reacts with the manganese peroxo species by nucleophilic attack, then OPD is oxidized to form the OPD^{*+} species and the color changes to orange. The function of the BSA-MnO_2 NPs is to accelerate the electron-transfer process and the consequent facilitation of radical generation. For the TMB oxidation, the K_m of BSA-MnO_2 NPs was smaller than that of Fe_3O_4 NPs[8] and CeO_2 NPs,[23] indicating that the affinity between TMB and BSA-MnO_2 NPs is stronger than that between TMB and Fe_3O_4 NPs and TMB and CeO_2 NPs. Furthermore, the V_{max} of BSA-MnO_2 NPs with TMB was larger than that of Fe_3O_4 NPs by two orders of magnitude and of CeO_2 NPs by one order of magnitude. These showed that the BSA-MnO_2 NPs have a higher oxidase-like activity in the absence of H_2O_2. In addition, the K_{cat} values of BSA-MnO_2 NPs with OPD substrate, H_2O_2 substrate and TMB substrate were larger than HRP, indicating that at the same molar concentration, the catalytic efficiency of BSA-MnO_2 NPs was higher than HRP.

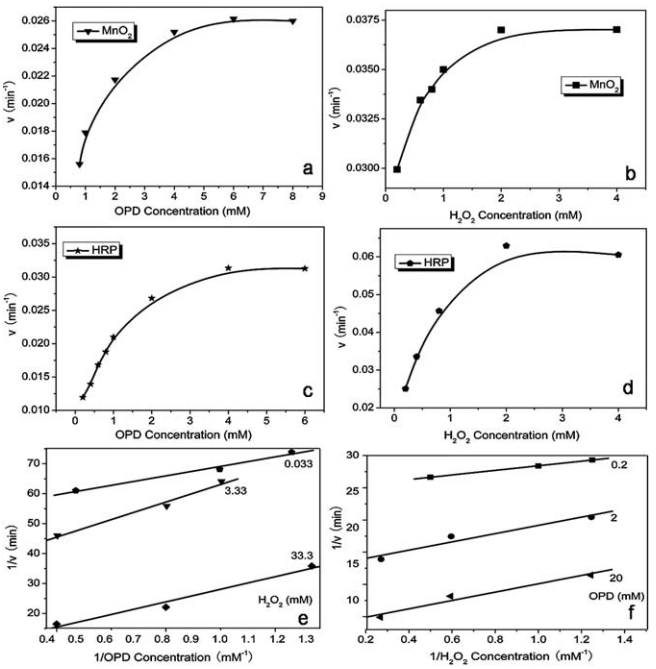

Fig. 3 Steady-state kinetic assays of BSA-MnO_2 NPs with OPD oxidation (a–f). The velocity (v) of the reaction was measured using 3.7 μg mL^{-1} BSA-MnO_2 NPs (a and b) and 3.3 μg mL^{-1} HRP (c and d) in 300 μL NaAc buffer at pH 4.0 and temperature 35 °C. (a and c) The concentration of H_2O_2 was 3.3 mM for BSA-MnO_2 NPs or 0.3 mM for HRP and the OPD concentration was varied; (b and d) the concentration of OPD was 0.17 mM and the H_2O_2 concentration was varied; and (e and f) double reciprocal plots of activity of BSA-MnO_2 NPs with the concentration of one substrate (H_2O_2 or OPD) fixed and the other varied.

3.7. Detection of H_2O_2

The color variation of TMB oxidation catalyzed by MnO_2 NPs was MnO_2 concentration-dependent. The absorbance at 652 nm

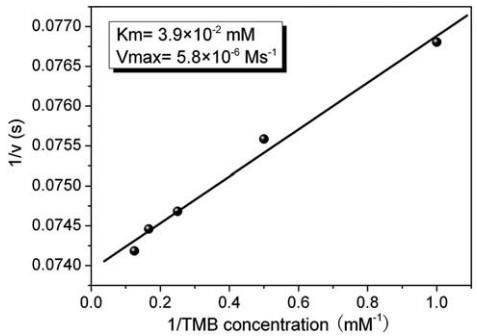

Fig. 4 Steady-state kinetic assay of BSA-MnO_2 NPs with TMB oxidation. The velocity (v) of the reaction was measured using 3.7 μg mL^{-1} BSA-MnO_2 NPs in 300 μL citrate buffer at pH 4.0 and temperature 35 °C.

Table 1 Comparison of the kinetic parameters between BSA-MnO_2 NPs and HRP. [E] is the BSA-MnO_2 NPs (or HRP) concentration, K_m is the Michaelis–Menten constant, V_{max} is the maximal reaction rate and K_{cat} is the catalytic constant, where $K_{cat} = V_{max}/[E]$. Experimental conditions were under standard conditions

Catalyst	Substrate	[E]/M	K_{cat}/s^{-1}	K_m/mM	$V_{max}/10^{-8}$ M s^{-1}
MnO_2	OPD	3.01×10^{-8}	2.728	0.31	8.21
MnO_2	H_2O_2	3.01×10^{-8}	1.897	0.12	5.71
HRP	OPD	8.25×10^{-8}	0.564	0.59	4.65
HRP	H_2O_2	8.25×10^{-8}	1.149	0.34	9.48
MnO_2	TMB	3.01×10^{-8}	192.0	0.04	578
Fe_3O_4	TMB	1.14×10^{-12}	3.02×10^4	0.098	3.44
CeO_2	TMB	—	—	3.8	70

was proportional to MnO_2 concentration from 0.00016 to –0.016 mM with a detection limit (DL) of 5.9×10^{-8} M and the color variation was obvious on visual observation (Fig. S12, inset, ESI†). The color variation of OPD oxidation catalyzed by MnO_2 NPs was H_2O_2 concentration-dependent. This indicated that the absorbance change can be used for the detection of H_2O_2. It showed the standard curve with the linear range for H_2O_2 was from 0.016 to 333 mM and the DL was as low as 0.01 mM (Fig. S13, ESI†).

3.8. Application in immunoassay

Since the catalytic activity originates from MnO_2, the as-synthesized BSA-MnO_2 NPs provide excellent availability for bioconjugation without losing their catalytic activity, which is extremely important for typical labeled bioassays. Both peroxidase- and oxidase-like activities of BSA-MnO_2 NPs were tested in colorimetric immunoassay for the detection of goat anti-human IgG as an example (Fig. 5a). Fig. 5b displayed that the absorbance at 450 nm of OPD was associated with the concentration of goat anti-human IgG in the presence of H_2O_2. The DL was 0.25 μg mL^{-1} with a linear range from 0.5 to 10 μg mL^{-1}. Fig. 5c displayed that the absorbance at 652 nm of TMB increased linearly with the concentration of goat anti-human IgG. The DL was 0.025 μg mL^{-1} with a linear range from 0.025 to 10 μg mL^{-1}. The colorimetric immunoassay using BSA-MnO_2 NPs has the advantages of being fast, robust, inexpensive, easily prepared, convenient, very efficient and that no HRP and H_2O_2 are needed, holding promising potential applications in facile and biocompatible labeling for sensitive and robust nano-biosensor development.

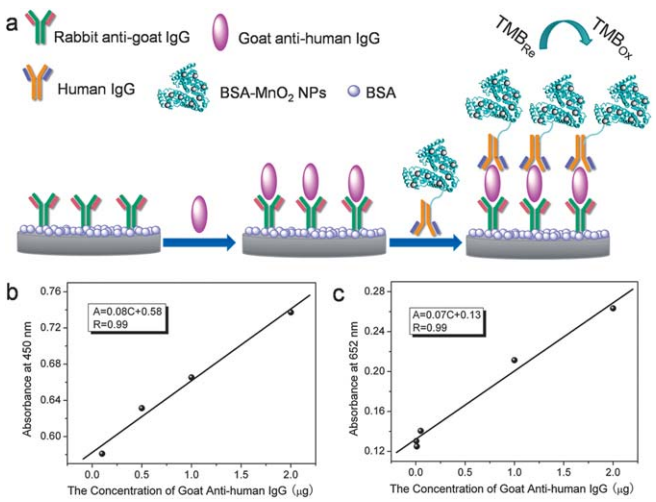

Fig. 5 (a) Schematic of using BSA-MnO_2 NPs as a sandwich immunoassay tags for goat anti-human IgG determination with TMB as substrate; a linear calibration plot for goat anti-human IgG detection with (b) H_2O_2 oxidation of OPD, and (c) dissolved oxygen oxidation of TMB.

4. Conclusions

In conclusion, small-sized MnO_2 NPs with a high enzyme activity were synthesized using the BSA template. We first found that the BSA-MnO_2 NPs possess high peroxidase-, oxidase- and catalase-like activities. The colorimetric immunoassay using BSA-MnO_2 NPs holds promising potential applications in biotechnology, bioassays, and biomedicine.

Acknowledgements

This work was supported by the National Natural Science Foundation of China (nos. 20835003 and 21075084) and the Sichuan Youth Science and Technology Foundation (no. 2009-18-409).

References

1 G. Liu, Y. Wan, V. Gau, J. Zhang, L. H. Wang, S. P. Song and C. H. Fan, *J. Am. Chem. Soc.*, 2008, **130**, 6820–6825.
2 F. Wen, Y. H. Dong, L. Feng, S. Wang, S. C. Zhang and X. R. Zhang, *Anal. Chem.*, 2011, **83**, 1193–1196.
3 P. Wu, Y. He, H. F. Wang and X. P. Yan, *Anal. Chem.*, 2010, **82**, 1427–1433.
4 Q. Zhao, X. F. Li and X. C. Le, *Anal. Chem.*, 2011, **83**, 9234–9236.
5 G. Philip, *Nature*, 1952, **169**, 612–613.
6 Z. Lin, W. Xue, H. Chen and J. M. Lin, *Anal. Chem.*, 2011, **83**, 8245–8251.
7 C. J. Mao, Y. X. Zhao, X. F. Qiu, J. J. Zhu and C. Burda, *Phys. Chem. Chem. Phys.*, 2008, **10**, 5633–5638.
8 L. Z. Gao, J. Zhuang, L. Nie, J. B. Zhang, Y. Zhang, N. Gu, T. H. Wang, J. Feng, D. L. Yang, S. Perrett and X. Y. Yan, *Nat. Nanotechnol.*, 2007, **2**, 577–583.
9 R. André, F. Natálio, M. Humanes, J. Leppin, K. Heinze, R. Wever, H. C. Schröder, W. E. G. Müller and W. Tremel, *Adv. Funct. Mater.*, 2011, **21**, 501–509.
10 J. Fan, J. J. Yin, B. Ning, X. C. Wu, Y. Hu, M. Ferrari, G. J. Anderson, J. Y. Wei, Y. L. Zhao and G. J. Nie, *Biomaterials*, 2011, **32**, 1611–1618.
11 J. B. Liu, X. N. Hu, S. Hou, T. Wen, W. Q. Liu, X. Zhu and X. C. Wu, *Chem. Commun.*, 2011, **47**, 10981–10983.
12 Y. Jv, B. X. Li and R. Cao, *Chem. Commun.*, 2010, **46**, 8017–8019.

13 Y. J. Long, Y. F. Li, Y. Liu, J. J. Zheng, J. Tang and C. Z. Huang, *Chem. Commun.*, 2011, **47**, 11939–11941.
14 W. B. Shi, Q. L. Wang, Y. J. Long, Z. L. Cheng, S. H. Chen, H. Z. Zheng and Y. M. Huang, *Chem. Commun.*, 2011, **47**, 6695–6697.
15 Y. Song, K. Qu, C. Zhao, J. Ren and X. Qu, *Adv. Mater.*, 2010, **22**, 2206–2210.
16 Y. J. Song, X. H. Wang, C. Zhao, K. G. Qu, J. S. Ren and X. G. Qu, *Chem.–Eur. J.*, 2010, **16**, 3617–3621.
17 W. Chen, J. Chen, Y. B. Feng, L. Hong, Q. Y. Chen, L. F. Wu, X. H. Lin and X. H. Xia, *Analyst*, 2012, **137**, 1706–1712.
18 P. Roy, Z. H. Lin, C. T. Liang and H. T. Chang, *Chem. Commun.*, 2012, **48**, 4079–4081.
19 J. S. Mu, Y. Wang, M. Zhao and L. Zhang, *Chem. Commun.*, 2012, **48**, 2540–2542.
20 Y. Fan and Y. Huang, *Analyst*, 2012, **137**, 1225–1231.
21 S. Liu, J. Tian, L. Wang, Y. Luo, G. Chang and X. Sun, *Analyst*, 2011, **136**, 4894–4897.
22 Y. Zhang, J. Tian, S. Liu, L. Wang, X. Qin, W. Lu, G. Chang, Y. Luo, A. M. Asiri, A. O. Al-Youbi and X. Sun, *Analyst*, 2012, **137**, 1325–1328.
23 A. Asati, S. Santra, C. Kaittanis, S. Nath and J. M. Perez, *Angew. Chem., Int. Ed.*, 2009, **48**, 2308–2312.
24 J. J. Wang, X. G. Mi, H. Y. Guan, X. H. Wang and Y. Wu, *Chem. Commun.*, 2011, **47**, 2940–2942.
25 X. Q. Chen, X. Z. Tian, I. Shin and J. Yoon, *Chem. Soc. Rev.*, 2011, **40**, 4783–4804.
26 T. Porstmann and S. T. Kiessig, *J. Immunol. Methods*, 1992, **150**, 5–21.
27 A. Ambrosi, F. Airo and A. Merkoçi, *Anal. Chem.*, 2009, **82**, 1151–1156.
28 D. Porter and H. Bright, *J. Biol. Chem.*, 1983, **258**, 9913–9924.
29 S. J. Yao, J. H. Xu, Y. Wang, X. X. Chen, Y. X. Xu and S. S. Hu, *Anal. Chim. Acta*, 2006, **557**, 78–84.
30 J. P. Xie, Y. G. Zheng and J. Y. Ying, *J. Am. Chem. Soc.*, 2009, **131**, 888–889.
31 N. Goswami, A. Giri, M. S. Bootharaju, P. L. Xavier, T. Pradeep and S. K. Pal, *Anal. Chem.*, 2011, **83**, 9676–9680.
32 A. Retnakumari, S. Setua, D. Menon, P. Ravindran, H. Muhammed, T. Pradeep, S. Nair and M. Koyakutty, *Nanotechnology*, 2010, **21**, 055103.
33 X. Huang, H. Yue, A. Attia and Y. Yang, *J. Electrochem. Soc.*, 2007, **154**, A26–A33.

